Available online at www.sciencedirect.com
ScienceDirect
Journal of Electron Spectroscopy and Related Phenomena 162 (2008) 30–35
JOURNAL OF ELECTRON SPECTROSCOPY and Related Phenomena
www.elsevier.com/locate/elspec

Valence photoelectron spectrum of KBr: Effects of electron correlation

A. Caló *, M. Huttula, M. Patanen, H. Aksela, S. Aksela

Department of Physical Sciences, University of Oulu, P.O. Box 3000, Fin-90014 Oulu, Finland

Received 8 June 2007; received in revised form 10 August 2007; accepted 17 August 2007
Available online 23 August 2007

Abstract

The valence photoelectron spectrum has been measured for molecular KBr. Experimental energies of the main and satellite structures have been compared with the results of *ab initio* calculations based on molecular orbital theory including configuration and multiconfiguration interaction approaches. Comparison between the experimental KBr spectrum and previously reported Kr valence photoelectron spectrum has also been performed in order to find out if electron correlation is of the same importance in the valence ionized state of KBr as in the corresponding state of Kr.

PACS: 32.80.Hd

Keywords: KBr; Valence photoionization; Molecular calculations

1. Introduction

The physical and chemical properties of alkali halide molecules have been the subject of numerous investigations (see e.g. [1,2] and references therein) because of the ionic character of their molecular bond that allows the application of simple theoretical models. Most lately we studied both the electronic decay of the valence VUV resonances and also the Auger decay following the core ionization in either the alkali or the halide side of the molecule (see [1–4] and references therein). In the study of the Br normal Auger spectra (MNN) in the alkali bromide series [3], the experimental results were compared with the results of single configuration calculations for Br^-decay spectrum [5,6]. It was noticed that the molecular Auger decay resembles in great extend the decay in Br^-ions when the final state of the Auger transition involves the electrons from the outermost molecular orbitals (MOs) (4p in Br^-). However, great differences between the spectrum of Br^-ion and the alkali bromide spectra were seen in the Auger groups involving the inner valence (Br 4s) MO. Single configuration calculations for Br^- failed completely in describing the features of these Auger groups. It is known that electron correlation plays a dramatic role in the same Auger group of Kr, shifting the energies and redistributing the intensity between the main and satellite lines [7]. Valence photoelectron spectrum of Kr is also accompanied by a rich satellite structure, due to the many-electron effects related to the valence ionization (see ref. [8] and references therein). The study of the inner valence photoelectron spectra of the alkali bromides was thus assumed to provide information not only on the structure of the molecular orbitals but also on the Br MNN Auger final states.

The outer valence spectrum of KBr has been recorded earlier [9,10] with the HeI and HeII discharge lamp excitation, covering the spectral range of Br^- 4p and K^+ 3p orbitals. However, the existing data does not show any indications of the Br^- 4s or the K^+ 3s orbitals. As far as we know, no synchrotron radiation excited high resolution experiments for gas-phase KBr have been reported so far.

In the present study we have measured the synchrotron radiation excited molecular KBr valence photoelectron spectrum including the 4p and 4s orbitals of Br^- and also the 3p and 3s orbitals of K^+. We also investigated whether the valence photoelectron spectrum of Br^- reflects similar satellite structure as seen in the spectra of the isoelectronic Kr atom [8].

* Corresponding author. Tel.: +358 8 5531317; fax: +358 8 5531287.
E-mail address: antonio.calo@oulu.fi (A. Caló).

0368-2048/$ – see front matter © 2007 Elsevier B.V. All rights reserved.
doi:10.1016/j.elspec.2007.08.006

2. Computational details

Calculations were performed using the quantum chemistry software package GAMESS [11,12]. Configuration interaction (CI) [13] and multiconfigurational self-consistent field (MCSCF) [14–16] wavefunctions, in a full optimized reaction space (FORS), also known as complete active space (CASSCF), were adopted. Calculations including the spin-orbit (SO) interaction were not performed. While the use of the MCSCF calculations was favorable for the higher quality level of their results, the CI calculations turned out to be very useful because of their less demanding nature, allowing us to reach deeper photoionization levels within our memory and computational time limits. Through the Mulliken [17–21] and the Lowdin [22] population analysis we could estimate the atomic orbitals (AO) contribution for each MO. This allowed us to determine if and how the ionic character of the molecule changes across the studied range of MO, indicating possible limits of the ionic model. For K we used the Pople's 6-311** valence triple zeta with polarization basis set [23]. For Br the augmented Dunning type correlation consistent aug-cc-pVDZ [24] was used. The ionization energies (IE) have been calculated in the minimum of the potential energy curve (PEC) for the neutral KBr molecule, corresponding to a calculated internuclear distance of 2.915 Å, in nice agreement with previous evaluations [25].

3. Experiments

Measurements were performed at the beamline I411 [26] in MAX-laboratory in Lund, Sweden. The beamline uses synchrotron radiation of an undulator located at the 1.5 GeV MAX-II storage ring. A modified Scienta SES-100 electron spectrometer was used to record the spectra of the emitted electrons at the "magic" 54.7° angle from the polarization vector, corresponding to angle-independent measurements. For a detailed description of the electron energy analyzer see ref. [27]. The molecular beam of KBr was produced from solid KBr in stainless steel crucible using a computer controlled inductively heated oven, designed and built at the University of Oulu [28]. The temperature of the crucible in the measurements was around 500 ° C corresponding the vapor pressure of 10^{-2} mbar [29,30] inside the crucible. Temperature was controlled with thermocouple sensors connected to the oven. The photon energy of 61.5 eV was used in the measurements of the KBr valence photoelectron spectrum (PES). Also other photon energies (60, 66, 70 eV) were used to identify possible Auger transitions and second order contributions at the kinetic energy region of the measurements. The binding energy calibration of the KBr photoelectron spectrum was obtained by introducing Xe gas to the interaction region and recording the Xe 5p photolines at 12.130 and 13.436 eV binding energy [31] simultaneously with the spectrum of KBr. The KBr photoelectron spectrum was measured with 20 eV pass energy of the electron spectrometer corresponding to approximately 70 meV analyzer contribution to the linewidths. The photon bandwidth was estimated to be 40 meV with the 100 μm exit slit of the monochromator.

4. Results and discussion

The valence photoelectron spectrum of KBr is presented in Fig. 1. The main KBr related structures are seen at the binding energies around 9, 19, 25 and 41 eV. In addition to the structures related to the inner and outer valence orbitals of KBr, the spectrum also includes some contributions related to the evaporation of background gases from the oven construction. The main residuals have been identified [32] to originate from CO_2 but small contributions of H_2O and CO have also been noticed.

Experimental and theoretical results are summarized in Tables 1–3 . In order to provide a systematic assignment for the whole range of experimental findings, we have used molec-

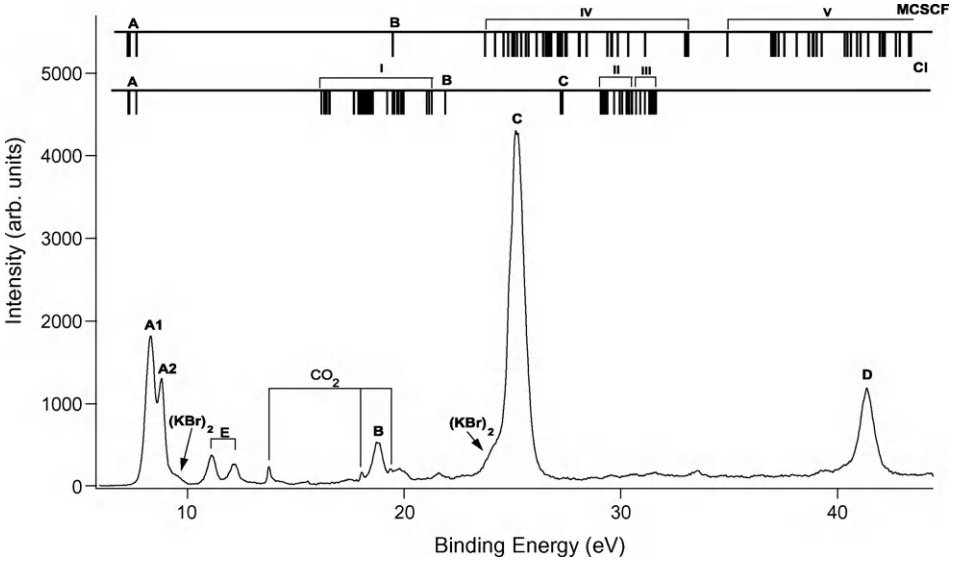

Fig. 1. Valence photoelectron spectrum of KBr molecule measured at 61.5 eV. In the top of the figure we schematically reported the results from the theoretical calculations.

Table 1
Comparison between the experimental values and the theoretical results from CI and MCSCF calculations for the main photolines

	Configuration	Exp.	CI	MCSCF	MCSCF + SO [a]	Leading contr.
A$_1$	$4\sigma^1 2\pi^4$ $4\sigma^2 2\pi^3$	8.29	7.26-7.31	7.25-7.32	7.07 ($^2\Sigma_{1/2}$) 7.25 ($^2\Pi_{3/2}$)	$Br^-(4p)^{-1}$
A$_2$	$4\sigma^2 2\pi^3$	8.80	7.63	7.64	7.89 ($^2\Pi_{1/2}$)	$Br^-(4p)^{-1}$
B	$3\sigma^1 4\sigma^2 2\pi^4$	18.84	21.90	19.48		$Br^-(4s)^{-1}$
C	$2\sigma^1 1\pi^4 3\sigma^2 4\sigma^2 2\pi^4$ $2\sigma^2 1\pi^3 3\sigma^2 4\sigma^2 2\pi^4$	25.17	27.22-27.30			$K^+(3p)^{-1}$
D	$1\sigma^1 2\sigma^2 1\pi^4 3\sigma^2 4\sigma^2 2\pi^4$	41.35	48.18			$K^+(3s)^{-1}$

[a]Results from "model calculations" (see text for details).

Table 2
Theoretical results for the satellite states from CI calculations

Label	Configuration	Energy	Leading atomic contr.
I	$4\sigma^1 2\pi^3\ 5\sigma^1$ $4\sigma^2 2\pi^2\ 5\sigma^1$ $4\sigma^1 2\pi^3\ 6\sigma^1/3\pi^1$ $4\sigma^2 2\pi^2\ 6\sigma^1/3\pi^1$	16.17-21.28	$K(4s)^{+1}Br^-(4p)^{-2}$ $Br^-(4p)^{-2}(5p)^{+1}$
II	$2\sigma^1 1\pi^4 3\sigma^2 4\sigma^2 2\pi^3\ 5\sigma^1$ $2\sigma^1 1\pi^4 3\sigma^2 4\sigma^1 2\pi^4\ 5\sigma^1$ $2\sigma^2 1\pi^3 3\sigma^2 4\sigma^2 2\pi^3\ 5\sigma^1$ $2\sigma^2 1\pi^3 3\sigma^2 4\sigma^1 2\pi^4\ 5\sigma^1$ $2\sigma^2 1\pi^4 3\sigma^1 4\sigma^2 2\pi^3\ 5\sigma^1$ $2\sigma^2 1\pi^4 3\sigma^1 4\sigma^1 2\pi^4\ 5\sigma^1$	29.07-30.53	$K^+(3p)^{-1}(4s)^{+1}Br^-(4p)^{-1}$ $K^+(4s)^{+1}Br^-(4s)^{-1}(4p)^{-1}$
III	$3\sigma^1 4\sigma^2 2\pi^3\ 6\sigma^1/3\pi^1$ $3\sigma^1 4\sigma^1 2\pi^4\ 6\sigma^1/3\pi^1$ $3\sigma^2 4\sigma^1 2\pi^2\ 5\sigma^2$ $3\sigma^2 4\sigma^2 2\pi^1\ 5\sigma^2$ $3\sigma^2 4\sigma^0 2\pi^3\ 5\sigma^2$	31.11-31.83	$Br^-(4s)^{-1}(4p)^{-1}(5p)^{+1}$ $K^+(4s)^{+2}Br^-(4p)^{-3}$

The states indicated with roman numbers refer to figure 1.

ular notation for the KBr^+MO as shown in Fig. 2. Although this scheme has no quantitative relevance, it is based on the Mulliken population analysis of the MCSCF calculations and it can provide a better understanding of the structure of the MO as they are mentioned in tables. According to the Lowdin and Mulliken population analysis the CI calculations were better able to describe the more covalent character of the Rydberg orbitals as compared to the MCSCF calculations because of the limited amount of excited configurations we could include in this heavier computation. This affected especially the results of the satellite states where the weight of the configuration with excited orbitals is more relevant.

Table 3
Theoretical results for the satellite states from MCSCF calculations

Label	Configuration	Energy	Leading atomic contr.
IV	$4\sigma^1 2\pi^3\ 3\delta^1$ $4\sigma^2 2\pi^2\ 3\delta^1$	23.73-33.10	$Br^-(4p)^{-2}(4d)^{+1}$
V	$3\sigma^1 4\sigma^2 2\pi^3\ 3\delta^1$ $3\sigma^1 4\sigma^1 2\pi^4\ 3\delta^1$	34.92-45.90	$Br^-(4s)^{-1}(4p)^{-1}(4d)^{+1}$

The states indicated with roman numbers refer to figure 1.

4.1. Main valence photolines

A summary of the theoretical and experimental results from the main photolines is shown in Table 1. The double peak structure indicated as A_1 and A_2 in Fig. 1 was first tentatively identified as $2\pi^{-1}$ and $4\sigma^{-1}$ MO, respectively, originating, according to the CI and MCSCF calculations, mainly from Br 4p orbitals

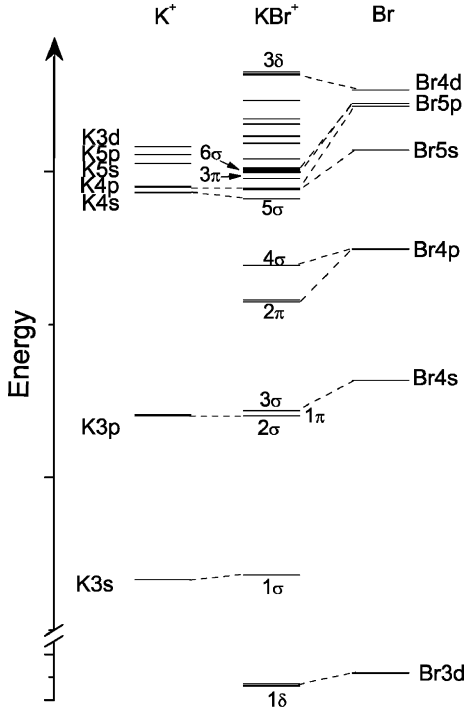

Fig. 2. MCSCF results for the contributions of the main atomic orbitals for the valence molecular orbitals of KBr.

[33,34]. Spin-orbit splitting of the Br $4p^{-1}$ state is, however, of the same order of magnitude as the splitting of the peaks A_1 and A_2, which is why the peaks most probably are of $4p_{3/2}{}^{-1}$ and $4p_{1/2}{}^{-1}$ character, respectively. As spin-orbit interaction was omitted in the calculations, both CI and MCSCF approximations fail in reproducing the splitting correctly. Using *model calculations* similar to [35] and SO splitting of 0.66 eV of Kr [36] we obtained 7.07 eV and 7.25 eV for $^2\Sigma 1/2$ and $^2\Pi 3/2$ molecular states (respectively), and 7.89 eV for $^2\Pi 1/2$. These results explain the broader and more intense A_1 peak as it is the result of two overlapping peaks.

The peak B at binding energy of 18.84 eV has been assigned to the $3\sigma^{-1}$ photoline originating mainly from Br 4s orbital. This structure was found to be partially overlapping with CO_2 photolines and KBr satellite structures. A detail of the 17–23 eV binding energy range shown in Fig. 3 will be discussed in more detail in chapter B below. The strongest structure C at 25.17 eV has been identified as the overlapping contributions of $1\pi^{-1}$ and $2\sigma^{-1}$ MO, originating mainly from K 3p orbitals [34]. Spin-orbit splitting of the K $3p^{-1}$ state is of minor importance, 0.18 eV [36], too small for a direct comparison as we did for the Br 4p-like signal. Nevertheless we can assume that the SO effect can in this case contribute to the broadening of peak C.

The dimer contribution, weak but clearly visible as indicated in Fig. 1, known for the alkaline part of the spectrum [33], appears on the higher binding energy side of the Br 4p line (A_1 and A_2 in Fig. 1). A similar contribution is believed to be visible on the lower binding energy side of the K 3p peak (C in Fig. 1). The reason of the different directions of the ionization energy shifts (monomer to dimer) in the halogen and alkali systems, is thought to be directly related to the ionic nature of the bonding characterizing the molecule. The Mulliken and Lowdin population analysis showed a partial negative (positive) charge of 0.9 e on the bromine (potassium) atom. Moving from monomer to dimer structure has probably an effect equivalent to a decreasing of the charge localized on each atom. The overall effect is to make the atoms less ionic and to consequently shift the ionization energies toward the levels for the neutral atom. In case of bromine, the shift is expected to be toward higher binding energies, being "easier" to ionize the Br^- ion than the Br neutral atom. Analogously the situation is expected to be the opposite for potassium where the shift is toward the lower ionization energy being "easier" to ionize the K neutral atom than the K^+ ion.

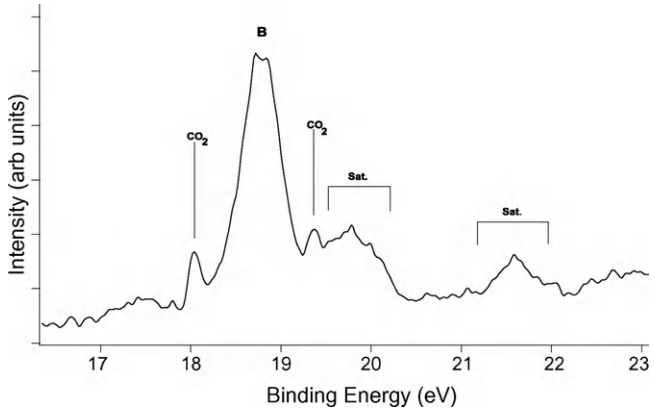

Fig. 3. Valence photoelectron spectrum of KBr in the 16.5–23 eV binding energy region.

The so far unreported mostly K 3s like $1\sigma^{-1}$ MO has been indicated as D in Fig. 1 at 41.35 eV. The double peak structure at 11.1 and 12.1 eV indicated as E in Fig. 1 has been identified as Br 3d photolines arising from the small second order contribution of the monochromator (123 eV). The binding energy has been evaluated to be 72.65 eV (Br $3d_{3/2}$) and 73.65 eV (Br $3d_{1/2}$ eV) in nice agreement with our earlier theoretical calculations [3] where the Br 3d ionization energies in KBr where predicted at 73.41 and 74.55 eV. As far as we know, the Br 3d lines of KBr have not been reported earlier.

As seen from Table 1 the theoretical results show a better correspondence with experiment for the outer valence shells compared to the inner shells. As we would expect, the MCSCF calculations provide more accurate results compared to the CI calculations. The advantage of the CI calculations was that their less demanding nature allowed us to include a higher number of configurations compared to the MCSCF approach, i.e. the 1σ and 2σ (respectively potassium 3s and 3p like orbitals, see Fig. 2) allowing us to reach deeper ionized states. However, the binding energies of the deeply ionized states were overestimated by the CI calculations, with the energy differences increasing with the binding energy. This indicates that electron correlation is not correctly accounted for in the CI approximation. The finding that calculations fail to fully reproduce the experiment is in agreement with Kr valence photoionization [7], where the predictions for the inner valence hole states were seen to strongly depend on the configuration set included in the calculations.

4.2. Satellite lines

We present here the theoretical results in Table 2 and 3 for the satellite states indicated with roman numbers in Fig. 1 in the two sets of results from the CI and MCSCF calculations. In the tables the main configuration is indicated, but most of the states were seen to be strongly mixed with other configuration states.

The Br^- and K^+ ions are isoelectronic with Kr and Ar respectively. We may thus expect some correspondence between the KBr and the Kr valence PES. In a previous work [8] we conducted a detailed analysis of the Kr satellite lines below the Kr 3d threshold, identifying a number of lines of the complex satellite structure that lies across the 28–40 eV binding energy region next to the Kr 4s photoline (25.5 eV) due to many-electron processes accompanying the valence photoionization. The lines were classified as monopole shake up (dipole photoionization accompanied by monopole excitation) and conjugated shake up (monopole photoionization accompanied by dipole excitation). In addition to these shake up satellites a series of intense correlation satellites, originating from the mixing between the Kr $4s^{-1}$ valence hole configuration and the

two-hole-one-electron configurations $4p^{-2}5s$ and $4p^{-2}4d$, were observed.

For KBr, the theoretical results from CI calculations (group I in Table 2) may find clear experimental evidence in the pronounced satellite structure present in the 17–23 eV binding energy region shown in Fig. 3. The corresponding two-valence-hole-states $(4\sigma 2\pi)^{-2}$– but with the excited electron on the 3δ orbital instead of on the 5σ one – are predicted by MCSCF calculations to lie at somewhat higher energy (group IV in Table 3). The shift to higher energies is most probably related to the fact that we had to limit the number of excited contributions in the MCSCF calculations. In contrast with the results for the main photolines shown in the previous section, now the experimental spectrum is better described by the CI calculations where the included excited configurations played and important role. Based on the comparison between the experiment and theory, we conclude that a similar two-hole-one-electron CI satellite structure as in Kr 4s photoelectron spectrum [8] also appears in the spectrum of KBr. Actually the whole binding energy range of 17–40 eV of Fig. 1 displays a background due to a multitude of weak structures, most probably created by satellite transitions. In Kr, the CI satellites with pronounced $4p^{-2}nl$ character were seen to cover a long energy range as the *nl* electron occupies a long ranging set of Rydberg orbitals n s and $(n-1)$ d $(n = 5, 6\ldots)$.

The satellite structure indicated as group II and III in Table 2 and as group V in Table 3 are monopole shake up satellite states. In analogy to the Kr case, we expect this kind of structures to be much weaker compared to the CI satellites structures. In KBr valence spectrum of Fig. 1 we may assign part of the weak satellite structures in the 28–40 eV binding energy region to be created by shake up satellite transitions. Also in this case the MCSCF calculations show a tendency to overestimate the satellite binding energies.

5. Conclusions

The valence photoelectron spectrum of KBr has been studied. The theoretical results have been shown to be in fairly good agreement with the experiment. The results reflected the different capabilities of the two used computational approaches in describing the highly excited molecular states, with the MCSCF calculations proving to be more effective in the description of the main valence photolines while the CI calculations where better in describing the excited MO characterizing the satellite structures. In this regard the ionic description of the KBr molecule turned out to be no longer appropriate for the two-hole-one-electron configurations with the outermost electron on a high Rydberg orbital.

Acknowledgments

This work has been supported by the Research Council for the Natural Science of the Finnish Academy, the Tauno Töning foundation and the European Community - Research Infrastructure Action under the FP6 “Structuring the European Research Area” Program (through the Integrated Infrastructure Initiative “Integrating Activity on Synchrotron and Free Electron Laser Science”). The authors would like to thank the staff of MAX-laboratory for the assistance during the measurements. We would like to thank also Edwin Kukk for the useful discussions and advises.

References

[1] E. Kukk, M. Huttula, H. Aksela, S. Aksela, E. Nõmmiste, A. Kikas, J. Phys. B. 36 (2003) 85.
[2] E. Kukk, M. Huttula, J. Rius, I. Riu, H. Aksela, S. Aksela, J. Phys. B. 37 (2004) 2739.
[3] Z.F. Hu, A. Caló, E. Kukk, J. Nikkinen, H. Aksela, S. Aksela, Chem. Phys. 121 (2004) 8246.
[4] Z.F. Hu, A. Caló, E. Kukk, H. Aksela, S. Aksela, J. Chem. Phys. 313 (2005) 77.
[5] K.G. Dyall, I.P. Grant, C.T. Johnson, F.A. Parpia, Comput. Phys. Commun. 55 (1989) 425.
[6] F.A. Parpia, C. Froese Fischer, I.P. Grant, Comput. Phys. Commun. 94 (1996) 249;
I.P. Grant, Relativistic Atomic Structure, in Atomic, Molecular and Optical Physics Reference Book, ed. G.W.F. Drake (American Institu of Physics, New York, 1996) ch. 22, 258–286.
[7] H. Aksela, S. Aksela, H. Pulkkinen, Phys. Rev. A: At. Mol. Opt. Phys. 30 (1984) 2456.
[8] A. Caló, S. Atanassova, R. Sankari, A. Kivimaki, H. Aksela, S. Aksela, J. Phys. B 39 (2006) 4169.
[9] A.W. Potts, W.C. Price, Phys. Scripta 16 (1977) 191.
[10] R.T. Poole, R.C.G. Leckley, J.G. Jenkin, J. Liesegang, Chem. Phys. Lett. 31 (1975) 308.
[11] M.W. Schmidt, K.K. Baldridge, J.A. Boatz, S.T. Elbert, M.S. Gordon, J.H. Jensen, S. Koseki, N. Matsunaga, K.A. Nguyen, S.J. Su, T.L. Windus, M. Dupuis, J.A. Montgomery, J. Comput. Chem. 14 (1993) 1347.
[12] M.S. Gordon and M.W. Schmidt, Eds. Advances in electronic structure theory: GAMESS a decade later in Theory and Applications of Computational Chemistry, the first forty years (G. E. Scuseria, Elsevier, Amsterdam, 2005).
[13] J. Ivonic, K. Ruedenberg, Theor. Chem. Acc. 106 (2001) 339.
[14] M.R. Hoffman, D.J. Fox, J.F. Gaw, Y. Osamura, Y. Yamaguchi, R.S. Grev, G. Fitzgerald, H.F. Schaefer, P.J. Knowles, N.C. Handy, J. Chem. Phys. 80 (1984) 2660.
[15] Y. Yamaguchi, Y. Osamura, J.D. Goddard, H.F. Schaefer (Eds.), A New Dimension in Quantum Chemistry, Oxford Press, NY, 1994.
[16] T.J. Dudley, R.M. Olson, M.W. Schmidt, M.S. Gordon, J. Chem. Phys. 27 (2006) 353.
[17] R.S. Mulliken, J. Chem. Phys. 23 (1955) 1833.
[18] R.S. Mulliken, J. Chem. Phys. 23 (1955) 1841.
[19] R.S. Mulliken, J. Chem. Phys. 23 (1955) 2338.
[20] R.S. Mulliken, J. Chem. Phys. 23 (1955) 2343.
[21] J. Pipek, P.Z. Mezey, J. Chem. Phys. 90 (1989) 4916.
[22] P.-O. Lowdin, Adv. Chem. Phys. 5 (1970) 185.
[23] J.-P. Blaudeau, M.P. McGrath, L.A. Curtiss, L. Radom, J. Chem. Phys. 107 (1997) 5016.
[24] A.K. Wilson, D.E. Woon, K.A. Peterson, T.H. Dunning Jr., J. Chem. Phys. 110 (1999) 7667.
[25] S.A. Rice, W. Klemperer, J. Chem. Phys. 27 (1957) 573.
[26] M. Bässler, A. Ausmees, M. Jurvansuu, R. Feifel, J.-O. Forsell, P. de Tarso Fonseca, A. Kivimäki, S. Sundin, S.L. Sorensen, R. Nyholm, O. Björneholm, S. Aksela, S. Svensson, Nucl. Instrum. Methods in Phys. A 469 (2001) 382.
[27] M. Huttula, S. Heinäsmäki, H. Aksela, E. Kukk, S. Aksela, J. Electron Spectrosc. Relat. Phenom. 156–158 (2007) 270.
[28] A. Mäkinen, Master Thesis, University of Oulu (2006).
[29] R.E. Honig, RCA Rev. 23 (1962) 567.
[30] R.E. Honig, D.A. Kramer, RCA Rev. 30 (1969) 285.

[31] Moore C.E., Ionization potentials and ionization limits derived from the analysis of optical spectra, US Govt. Printing Office, Washington DC. (1970).
[32] K. Kimura, S. Katsumata, Y. Achiba, T. Yamazaki, and S. Iwata, Handbookof He I Photoelectron Spectra of Fundamental Organic Molecules, Halsted, New York, 1981.
[33] A.W. Potts, T.A. Williams, W.C. Price, Proc. R. Soc. Lond. A 341 (1974) 147–161.
[34] A.W. Potts, T.A. Williams, J. Chem. Soc. Faraday Trans. 2 72 (1974) 1892–1900.
[35] R.F. Fink, M. Kivilompolo, H. Aksela, S. Aksela, Phys. Rev. 58 (1998) 1988–2000.
[36] C.E. Moore, Natl. Stand. Ref. Data Ser., Natl Bur. Stand. (U.S.) 35 (1971), I-III.